Desalination and Water Treatment
www.deswater.com

doi: 10.5004/dwt.2023.29907

307 (2023) 212–221
September

Decontamination of methylene blue and congo red by SCB/CuO nanocomposites: isotherms and kinetic studies

Shamroza Mubarik[a,*], Snovia Ali[a], Suryya Manzoor[b], Marryam Imran[a], Samreen Ehsan[a]

[a]*Department of Chemistry, Government Sadiq College Women University, Bahawalpur 63100, Pakistan, Tel.: +92 3227666144; emails: Shamroza.mubarik@gscwu.edu.pk (S. Mubarik), alisnovia@yahoo.com (S. Ali), Maryam.imranbwp@gmail.com (M. Imran), samreenehsan567@gmail.com (S. Ehsan)*
[b]*Institute of Chemical Sciences, Bahauddin Zakariya University, Multan, Pakistan, email: suryyia878@gmail.com*

Received 19 March 2023; Accepted 20 August 2023

ABSTRACT

In this study sugarcane bagasse copper oxide (SCB/CuO) nanocomposite was synthesized and its affinity for the batch adsorption of methylene blue and congo red was investigated. The impact of various operating factors including biosorbent dosage, contact time and pH on the percentage removal of these dyes was examined. The optimal contact time for methylene blue and congo red adsorption was 75 and 60 min, respectively. The optimum biomass dosage (SCB/CuO nanocomposite) for the decolorization of methylene blue and congo red was 0.02 and 0.04 g, respectively. The calculated value of zeta potential is 7. Second-order model was found to be most appropriate model for the elucidation of adsorption kinetics. Experimental results were established by applying various linear and non-linear isotherm models such as Langmuir, Freundlich, Temkin, Dubinin–Radushkevich, Halsey and Harkins–Jura etc. The obtained values of E according to Dubinin–Radushkevich is 1.9 and 13.86 kJ/mol for methylene blue and congo red, which showed physical and chemical nature of adsorption, respectively. The negative values of $\Delta G°$ and $\Delta H°$ indicated the spontaneity and exothermic nature of the process correspondingly.

Keywords: Adsorption; Pseudo-second-order; Linear isotherms; Methylene blue; Congo red; Sugarcane bagasse copper oxide (SCB/CuO) nanocomposite

1. Introduction

Urbanization and industrialization work together for supporting a peaceful and healthy living on earth. One of the main environmental issues associated with them is aquatic contamination brought about by the release of different heavy metals and dyes from diverse human activities [1,2]. The photosynthetic potential of aquatic plants may be impacted by the decreased solar light penetration caused by colored organic molecules in water [3]. The main causes of dyes' toxicity include various ingredients like aromatics and amines [4]. The majority of dyes have negative impact on human health, including kidney, liver, reproductive, and central nervous system malfunction, and are mutagenic, carcinogenic, or teratogenic to all living things [5]. These may harm the circulatory, digestive, and nervous systems, and may result in respiratory diseases, Parkinson's syndrome, multiple sclerosis, skin rashes, vomiting, and other unpleasant symptoms [6].

The researchers have extensively investigated cost-effective, environmentally acceptable, and sustainable methods for sequestering heavy metals and dyes from contaminated aquatic systems [7]. Traditional physical contamination removal techniques come in a variety of forms. Adsorption is a remediation technology that is effective, eco-friendly, simple to use, and affordable [8]. It can remove a variety of contaminants from wastewater, including organic, inorganic, and biological elements as well as soluble and insoluble

* Corresponding author.

chemicals [9]. Accessibility, low cost, non-hazardous, high adsorption capacity, high resistance to abrasion, and stability in various environmental conditions are some important qualities that an effective adsorbent should possess.

For the remediation of unclean water and soil systems, biochar, a carbon-rich and highly permeable adsorbent, has many applications [7]. The use of biochar as a sustainable, affordable, and environment friendly adsorbent made from various readily accessible agricultural byproducts has significantly advanced in recent years [10,11]. According to reports, the pyrolysis temperature and kind of material used to produce biochar determine the stability of the structure, the number of surface functional groups, and the adsorption capacity of the biochar [12,13].

Researchers are encouraged by the promise of environmentally friendly materials because of their increased effectiveness and cost-effectiveness [14]. Recent research has demonstrated that scientists have attempted to increase the efficiency of biochar by altering its surface properties through various changes using potent acids/bases, nanoparticles, etc. [15]. Successful applications of metal nanoparticles as adsorbents, reductants, oxidants, and catalysts have been made for a variety of pollutants, particularly heavy metals and dyes [2,16]. However, due to their aggregation/agglomeration, which results from the greater surface energy, metallic nanoparticles' high activity, and outstanding potential are occasionally diminished [17]. By reducing the agglomeration of metal nanoparticles and improving their surface properties, porous materials like biochar are used as excellent supports to increase their capacity to remove a variety of pollutants from the environment [18]. *Saccharum officinarum* grows by using solar energy through photosynthesis and thus producing biomass. Sugarcane is the crop with the highest biomass yield on an annual basis [19,20]. Annually, up to 8 tons of carbohydrate (sugar and bagasse) can be produced per acre [21]. Sugarcane is a fibrous plant, so the crushed remnants are thin, long particles that are intertwined with one another. As a result, bagasse has poor flow characteristics and tends to bunch together. Additional size reduction prior to pyrolysis will improve bagasse flow ability. Because of the porosity of the particles, determining the particle density of bagasse is particularly difficult. Bagasse is primarily composed of fiber particles with a high length-to-width ratio and small spongy dust-like particle [22]. The goal of the current research was to assess *Saccharum officinarum* biochar (SCB) for the treatment of dye and heavy metal-contaminated wastewater and to improve its properties using CuO metal nanoparticles.

2. Materials and methods

All the chemicals such as methylene blue (99%, Sigma-Aldrich, USA), congo red (99%, Sigma-Aldrich, USA), copper sulfate (99%, Sigma-Aldrich, USA), potassium hydroxide (99%, Sigma-Aldrich, USA) and other required reagents were purchased of analytical grade.

2.1. Adsorbate

The well–known cationic dye methylene blue is acquired from Sigma-Aldrich and employed as an adsorbent. Congo red is the sodium salt of benzidinediazo-bis-1-naphthylamine-4-sulfonic acid (formula $C_{32}H_{22}N_6Na_2O_6S_2$: molecular weight 696.66 g/mol). It was also purchased from Sigma-Aldrich. The stock solution of each dye was obtained by dissolving 1.0 g in 1 L of double distilled water and other necessary working solutions of these dyes were prepared by further dilution of the stock solutions. Fig. 1 depicts the molecular structure of methylene blue and congo red.

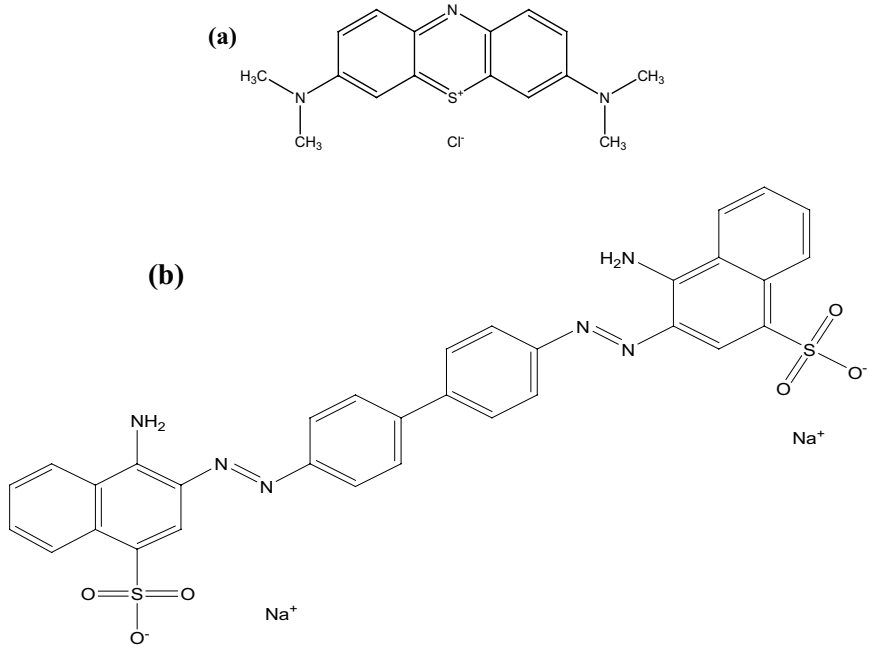

Fig. 1. Structure of (a) methylene blue and (b) congo red.

2.2. Adsorbents

2.2.1. Preparation of biochar

Sugarcane bagasse was collected from local sugarcane juice stall (Bahawalpur). The collected bagasse was washed 5–6 times with tap water and rinsed with distilled water. The rinsed bagasse was boiled in distilled water for 5–10 min for extra pureness. Pure form of boiled bagasse was then air dried for 2 d and pyrolyzed through slow pyrolysis at 500°C for 2–3 h in muffle furnace. Prepared biochar was crushed into powder with blender and sieved. The SCB was stored in a container for further use.

2.2.2. Preparation of nanocomposite

2.2.2.1. Copper oxide nanocomposite impregnated on sugarcane bagasse copper oxide (SCB/CuO)

30 mL of 0.1 M solution of copper sulfate pentahydrate ($CuSO_4 \cdot 5H_2O$) was taken into Erlenmeyer flask and 0.25 g of prepared biochar was added and the solution was shaken for 10 min on orbital shaker. Then the solution was titrated against 50 mL of 0.15 M solution of KOH by continuous stirring. Filtered the solution and dried the residue overnight at 70°C, scratched the dried residue and preserved for further use.

3. Results and discussion

3.1. Fourier-transform infrared spectroscopy studies

The Fourier-transform infrared (FTIR) spectra of biochar, and Cu–O nanocomposites are shown in the Figs. 2 and 3 in transmission mode from 600–4,000 cm^{-1}. FTIR spectra show the shift in transmission peaks caused by the material and its impregnation. In case of Cu–O nanocomposite spectrum, clear transmission peaks were observed at 3,588; 3,390; 2,160; 2,009; 1,990; 1,730; 1,559; 1,374; 1,339; 1,106; 980; 823 and 665 cm^{-1}. While SCB exhibited transmission peaks at 3,711; 3,014; 2,369; 2,124; 1,997; 1,822; 1,653; 1,636; 1,624; 1,617; 1,559 and 668 cm^{-1}. The –OH stretching vibrations occurred at transmission peaks 3,200–3,600 and 3,590 cm^{-1}

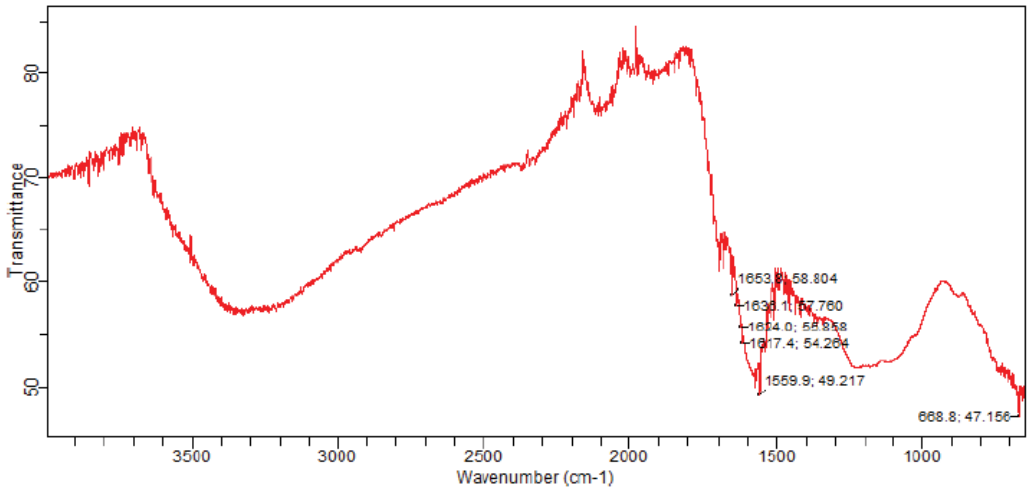

Fig. 2. Fourier-transform infrared spectrum of SCB.

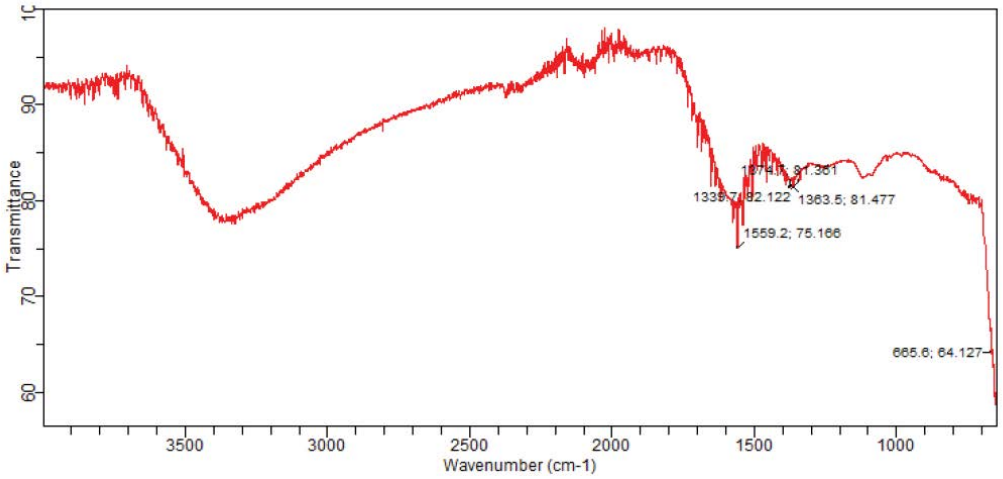

Fig. 3. Fourier-transform infrared spectrum of CuO/SCB nanocomposite.

whereas C–H stretching vibrations occurred at peaks 2,850–3,000 cm^{-1} indicating the weak signal. HC≡CH stretching vibrations at 2,300 cm^{-1}. Signal at 2,000–2,150 cm^{-1} indicated –C=C=C– functional group and – signal at 1,684 cm^{-1} indicated=O stretching vibration.

3.2. Scanning electron microscopy studies

The scanning electron microscopy images for the morphological features and surface characteristics of SCB/CuO nanocomposite are presented in Fig. 4. sugarcane bagasse

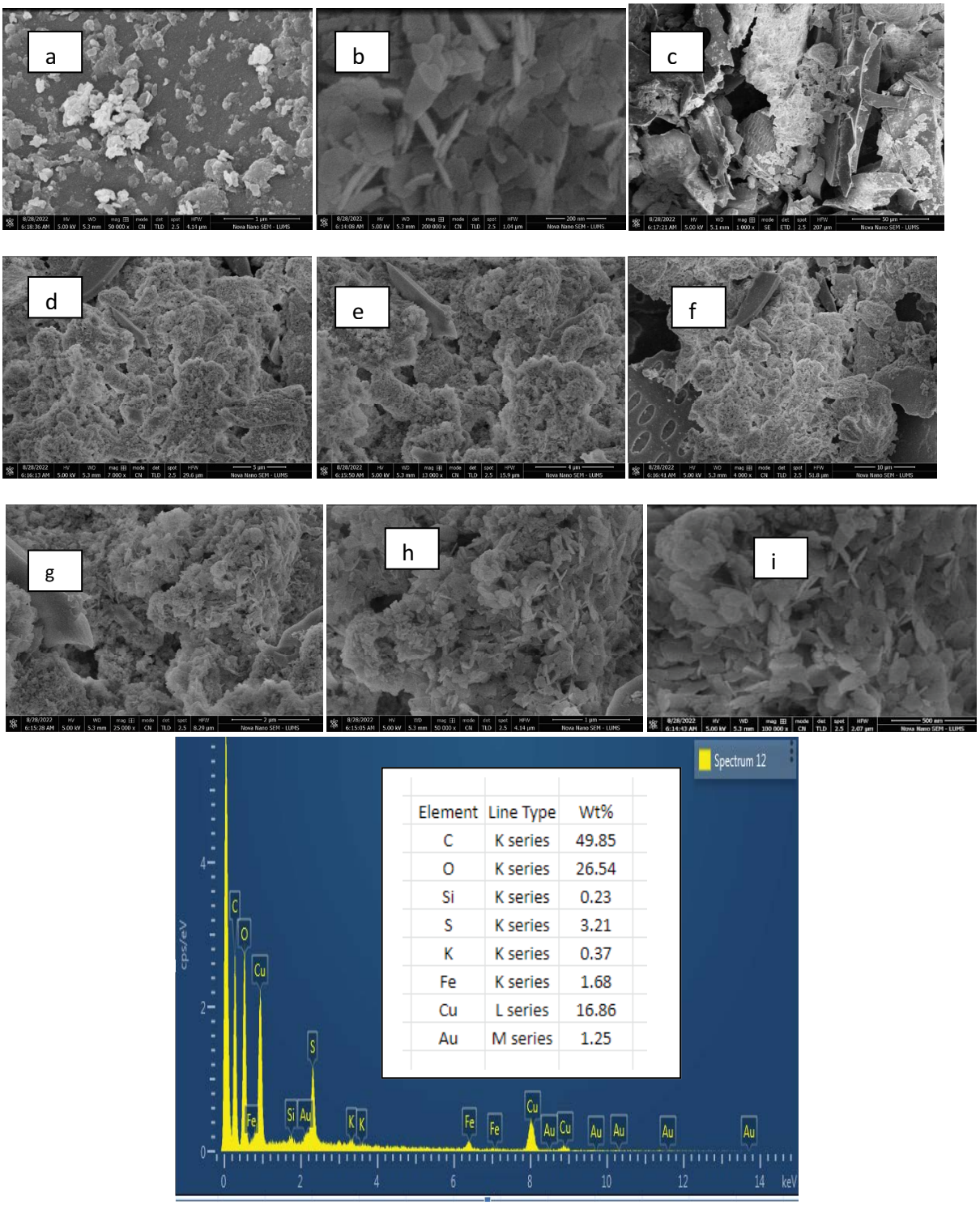

Fig. 4. (A) Scanning electron images of SCB/CuO nanocomposite and (B) energy dispersive X-ray spectrum of SCB/CuO nanocomposite.

copper oxide (SCB/CuO) nanocomposite has rough and irregular spaces with depressions on the surface which converted to smooth, long, deep well shaped micro tubes. Thus, rough and highly porous surface SCB/CuO nanocomposite facilitate the adsorption dyes by increasing the surface area.

3.3. Effect of operating factors

3.3.1. Batch binding assay

20 ppm solution of methylene blue and congo red solution was added with 0.5 g SCB/CuO nanocomposite. These systems were agitated on orbital shaker at 150 rpm for 6 h. The samples were collected into glass vials at every 15-min time interval. The obtained samples were then centrifuged at 4,000 rpm for 10 min. Absorbance of extracted samples were obtained at λ_{max}. Removal efficiency of these dyes can be assessed by UV–Vis spectrophotometer.

Batch binding assay was conducted to determine the matching degrees of binding sites.

Methylene blue revealed greater degree of binding affinity max. 94% while congo red showed comparatively less affinity max. 85% towards SCB/CuO nanocomposite (Fig. 5). Both dyes showed considerable binding affinity which means they have availability of complementary binding sites. The rapid increase in adsorption in the beginning is due to excessive availability of active sites but with the passage of time active sites became saturated and adsorption.

3.3.2. Effect of adsorbent dosage

It is important to determine the optimal dosage of adsorbents that minimizes the toxic substance to the lowest possible level for actual implementations and economic reasons. So that, the impact of dosage for the removal of dyes was determined by keeping other parameters constant. Fig. 5 reveals the potential of SCB/CuO nanocomposites for the removal of congo red and methylene blue when the adsorbent dosage was increased from 0.004 to 0.2 g/10 mL whereas other parameters remained constant. The data showed that there was significant increase in dyes removal with increasing the adsorbent dosage. The optimum adsorbent dosage for congo red and methylene blue was 0.04 and 0.02 g, respectively.

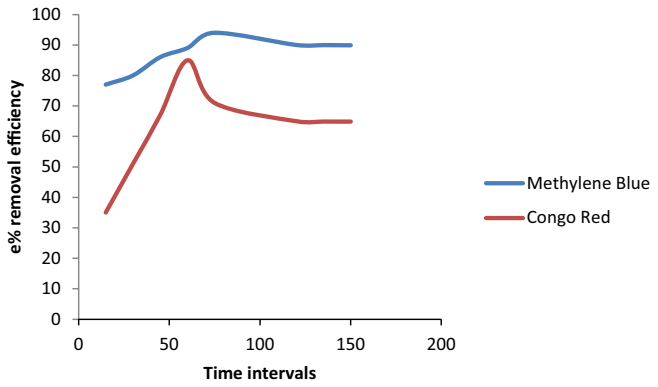

Fig. 5. Batch binding analysis of methylene blue and congo red by SCB/CuO nanocomposite.

3.3.3. Effect of concentration

Fig. 7 depicts the removal of dyes by SCB/CuO by varying the concentrations at the optimum dose of each adsorbent and ambient temperature. The data depicted the decline in the removal of dyes by the increase in concentration. The observed optimum concentration of methylene blue and congo red removal was 600 ppm.

3.3.4. Zeta potential

Fig. 8 depicts the value of pH_{PZC} for adsorbent is 7. At pH below 7 the surface of adsorbent has negative charge. Methylene blue is cationic dye so adsorbed at acidic dye While congo red is acidic so adsorbed at higher pH.

3.4. Adsorption kinetics

Kinetic models provide valuable information about equilibrium adsorption and clarify the mechanism of adsorption. In this study, experiments were done at room temperature. Two adsorption kinetic models including pseudo-first-order and pseudo-second-order were applied to study the kinetics of methylene blue and congo red on SCB/CuO (Fig. 10 and Table 1).

3.4.1. Pseudo-first-order model

The linearized pseudo-first-order reaction rate model can be given as:

$$\log\left(q_e - q_t\right) = \log q_e - k_1 T \tag{1}$$

The expression for non-linearized pseudo-first-order can be expressed as:

$$q_t = q_e\left(1 - e^{-k_1 T}\right) \tag{2}$$

where q_t and q_e describes the amount of adsorbed adsorbate at time t and at equilibrium, respectively and k_1 is the rate constant associated with first-order kinetic model.

The expression for linearized form of pseudo-second-order kinetic model can be showed by the following equation:

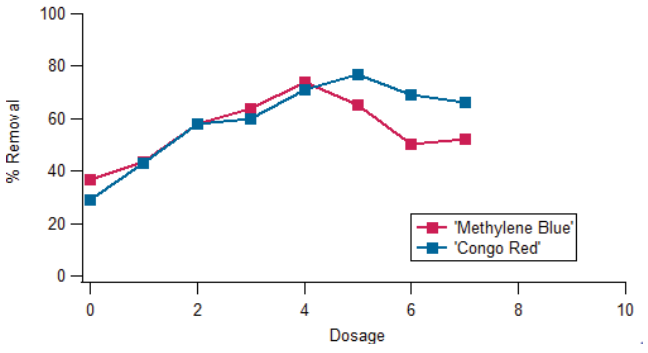

Fig. 6. Effect of dosage on the removal of methylene blue and congo red by SCB/CuO nanocomposite.

$$\frac{t}{q_t} = \frac{1}{k_2 q_e^2} + \frac{1}{q_e} \tag{3}$$

The non-linearized expression for pseudo-second-order can be demonstrated as:

$$q_t = \frac{K_2 q_e^2 t}{1 + K_2 q_e t} \tag{4}$$

where q_e is the quantity of adsorbate adsorbed at equilibrium and k_2 is the rate constant related to pseudo-second-order kinetic model.

The Weber and Morris intraparticle diffusion mode was used to elaborate the mechanism of adsorption.

$$q_t = Kt0.5 + I \tag{5}$$

Intercept of intraparticle diffusion model is not passing through origin which showed intraparticle diffusion model is taking part in the adsorption process.

3.5. Adsorption isotherms

3.5.1. Linear isotherms

The dyes removal performance of SCB/CuO was evaluated by applying isotherms. The equilibrium data of the study were analyzed with the models of Langmuir, Freundlich, Temkin, Dubinin–Radushkevich, and Halsey (Fig. 12).

The Langmuir isotherm is normally used to study the monolayer adsorption through homogeneous surfaces. Langmuir isotherm model discusses the relation between an adsorbed species and a sorbents system in which adsorbed species binding is limited to one molecular layer.

The expression for linear form can be given as:

$$\frac{1}{q_e} = \frac{1}{q_m} + \frac{1}{K_L q_m C_e} \tag{6}$$

where C_e is the concentration of adsorbate in solution at equilibrium, q_e refers to adsorbed adsorbate at equilibrium. K_L is Langmuir isotherm constant. A plot of C_e against C_e/q_e is given in Fig. 9a and values of the parameters K_L and q_m are listed in Table 2. R_L is a dimensionless separation factor and given as:

$$R_L = \frac{1}{1 + K_L C_0} \tag{7}$$

where C_o = maximum initial concentration of the adsorbate (mg/L).

If $R_L > 1$ then adsorption is unfavorable, if $R_L = 1$, $R_L = 0$, $0 < R_L > 1$ then adsorption is linear, irreversible and favorable, respectively.

Freundlich isotherm can be derived by assuming a decrease in logarithm in the adsorption enthalpy with the elevation of fractional occupied sites. The plot of logq_e vs. logC_e for linear form of equation yields the straight line as shown in Fig. 9b. The slope $1/n$ gives the information about the heterogeneity of the surfaces. The heterogeneity of the surfaces increased when the value of $1/n$ becomes closer to zero.

The linearized expression for Freundlich isotherm can be given as:

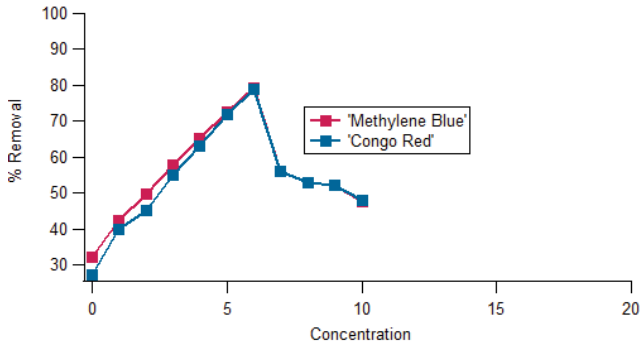

Fig. 7. Effect of concentration on the removal of methylene blue and congo red by SCB/CuO nanocomposite.

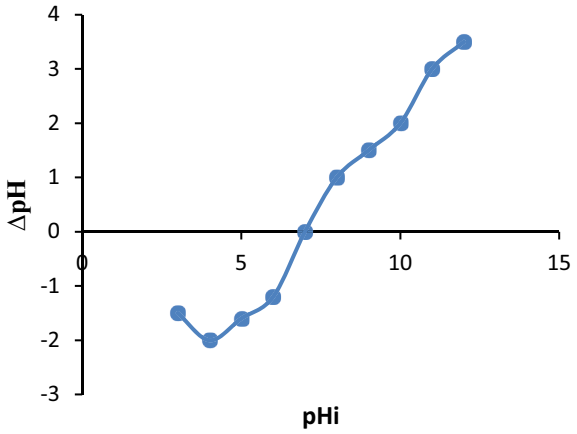

Fig. 8. Elucidation of surface charge through zeta potential.

Table 1
Parameters of pseudo-first-order and pseudo-second-order kinetic models for adsorption of methylene blue and congo red by SCB/CuO

System	Methylene blue	Congo red
	Pseudo-first-order	
k_1	0.002012	–0.000026
q_e	10.682222	1.675145
R^2	0.82	0.52
	Pseudo-second-order	
k_2	9,799.925	31.66748
q_e	62.5	7.262164
R^2	0.997	0.999
K	4.3	3.6
R^2	0.90	0.93
I	0.27	0.22

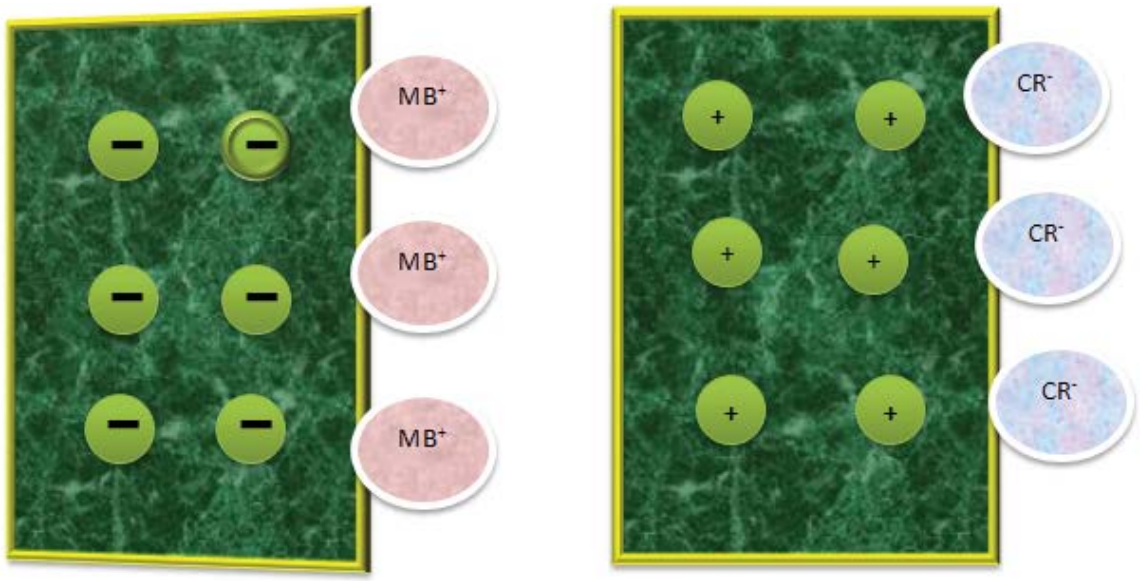

Fig. 9. Mechanism of adsorption of dyes on SCB/CuO nanocomposite.

Table 2
Parameters of the linear forms of Langmuir, Freundlich and Temkin isotherm for the adsorption methylene blue and congo red by SCB/CuO nanocomposite

System	Methylene blue	Congo red
	Langmuir	
q_m (mg/g)	-5×10^2	–270.27
K_L (mg/g)	-9.83×10^{-4}	-1.38×10^{-3}
	Temkin	
β (mg/L)	0.0057	0.0042
α (mg/L)	6.42680	6.8213
	Freundlich	
n_H	0.6145	0.6756
K (mg/L)	11.6546	6.0478
	Dubinin–Radushkevich	
B	0.1353	0.0026
q_m	2.28096	1.00682
E	1.9223	13.8675
	Halsey	
n_H	1.62733	1.480166
K_H	54.3894	14.3515

$$\ln q_e = \ln K_f + \frac{1}{n}\ln C_e \tag{8}$$

where K_f and n are Freundlich constant, the value of n provides information about heterogeneity the adsorbent surface. If the value of n is 2–10, then it reveals the decent adsorption power of the adsorbent. If it is 1–2, then it shows moderate adsorption and less than one signifies reduced adsorption capability.

The parameters of Freundlich isotherms are listed in Table 2 which revealed that Freundlich isotherm was well fitted.

The linear expression for Temkin isotherm can be given as:

$$Q_e = \frac{RT}{b_t}\ln A_t + \frac{RT}{b_t}\ln C_e \tag{9}$$

The model indicates the exothermic nature of adsorption reaction as $B > 0$ which is an indicator of release of heat during the process.

The following is the linear adsorption isotherm:

$$\log q_e = \frac{1}{nH\ln K_H} - \frac{1}{nH\log C_{\text{qe}}} \tag{10}$$

where K_H and n_H are the Halsey isotherm constants, which may be determined by plotting the slope and intercept of $\log q_e$ vs. $\log C_e$.

The Dubinin–Radushkevich isotherm is frequently used to demonstrate the process of adsorption onto a heterogeneous surface with a Gaussian energy distribution. The linear expression for Dubinin–Radushkevich can be given as:

$$\ln q_e = \ln q_m - B\varepsilon^2 \tag{11}$$

The expression for energy can be expressed as:

$$E = \frac{1}{\sqrt{2k_{\text{ads}}}} \tag{12}$$

The value of E calculated for the present research was 1.9 and 13.86 kJ/mol suggest physical nature of sorption for

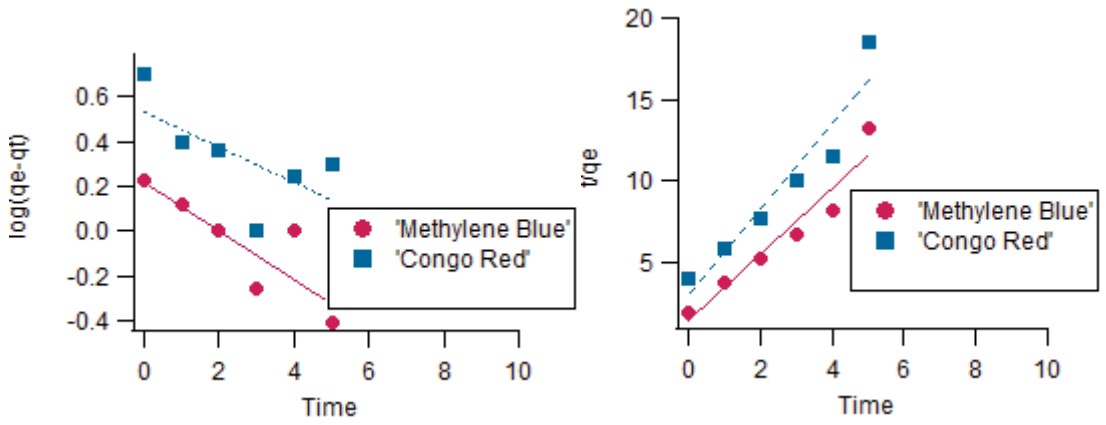

Fig. 10. Linear form of (a) pseudo-first-order kinetic model and (b) pseudo-second-order kinetic model for the adsorption of methyl blue and congo red by SCB/CuO nanocomposite.

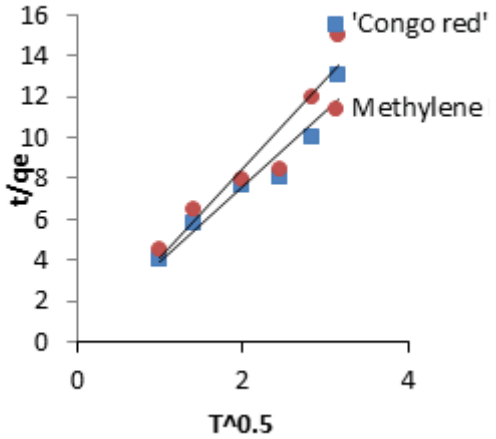

Fig. 11. Intraparticle diffusion kinetic plots for adsorption of methylene blue and congo red on SCB/CuO nanocomposite.

methylene blue and chemical nature for congo red. Because the value of E below 8 kJ/mol reflects physical sorption and 8–16 kJ/mol reflects chemical sorption.

3.5.2. Non-linear isotherms

The non-linear form of Langmuir isotherm can be expressed as:

$$q_e = \frac{q_m K_L C_e}{1 + K_L C_e} \tag{13}$$

where K_L is Langmuir constant, q_m is the adsorption capacity. The non-linear model of Langmuir isotherm is given in Fig. 13 and values of q_m and K_L are calculated in Table 3. The non-linear form of Freundlich can be represented:

$$q_e = K_F C_e \frac{1}{n} \tag{14}$$

where C_e is concentration of superflutant equilibrium stage, q_e is the quantity of dye adsorbed at equilibrium, n and K_f are Freundlich factors and their values are given in Table 3. The non-linear form of Temkin isotherm can be expressed as:

$$q_e = \frac{RT}{b_T \ln a_t C_e} \tag{15}$$

where R, T, b_T and a_t represent general gas constant, absolute temperature and heat of adsorption and equilibrium binding constant correspond to maximum binding energy, respectively. The expression for non-linear form of Temkin isotherm.

Table 3
Parameters of the non-linear forms of Langmuir, Freundlich and Temkin isotherms for the adsorption methylene blue and congo red by SCB/CuO nanocomposite

System	Methylene blue	Congo red
	Langmuir	
q_m (mg/g)	1.081e+006 ± 3.01e+007	1,338 ± 450
K_L (mg/g)	1.0992e-006 ± 3.1e-005	0.0011955 ± 0.000569
χ^2	0.377629	0.315306
	Temkin	
β (mg/L)	0.012612 ± 0.0012	0.012317 ± 0.000954
α (mg/L)	0.022402 ± 0.00366	0.02127 ± 0.00243
χ^2	0.324362	0.314875
	Freundlich	
N	1.1944 ± 0.187	1.2447 ± 0.144
K (mg/L)	2.9187 ± 2.25	3.4852 ± 1.9
χ^2	0.32732	0.319669
	Dubinin–Radushkevich	
$-B$	3,830.3 ± 795	2,917.4 ± 223
q_m	506.57 ± 30.5	498.68 ± 16.2
χ^2	0.317533	0.35658

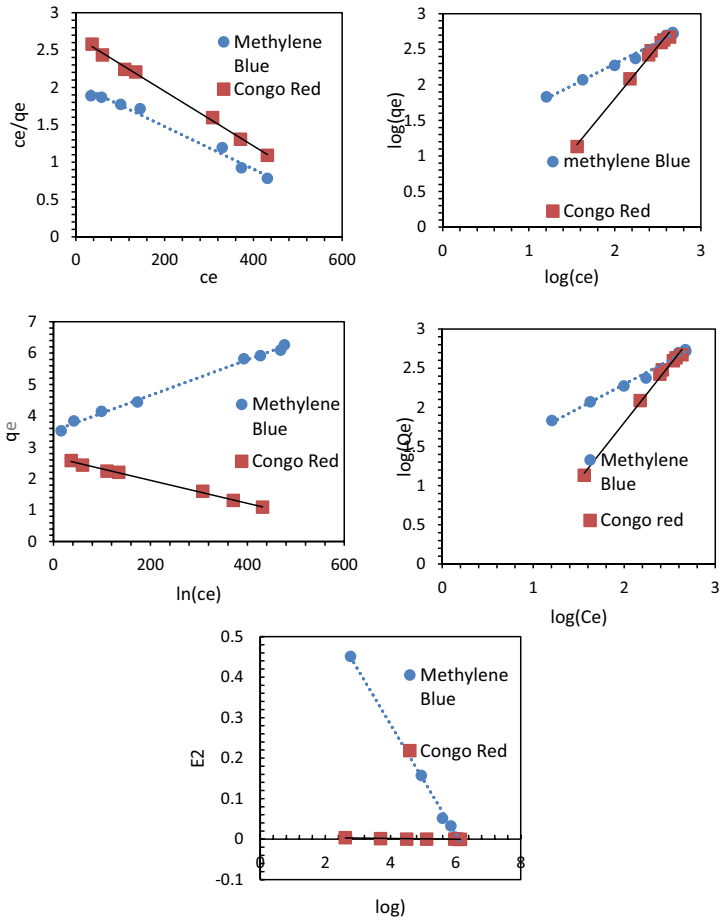

Fig. 12. Linear form of (a) Langmuir, (b) Freundlich, (c) Temkin, (d) Halsey and (e) Dubinin–Radushkevich for the adsorption of methylene blue and congo red by SCB/CuO nanocomposite.

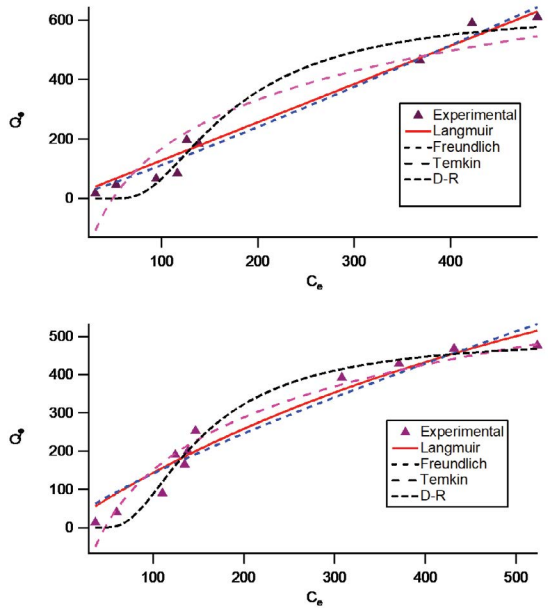

Fig. 13. Non-linear plots of Langmuir, Freundlich, Temkin, and Dubinin–Radushkevich isotherms for the adsorption of (a) methylene blue and (b) congo red by SCB/CuO nanocomposite.

Table 4
Thermodynamic parameters for adsorption methylene blue and congo red by SCB/CuO nanocomposite

Temperature	$\Delta G°$, kJ/mol	$\Delta H°$, kJ/mol	$\Delta S°$, J/mol·K
293	–0.06481		
303	–0.06702		
313	–0.06923	–0.00000831	0.026605
323	–0.07145		
333	–0.07366		

The non-linear form of Dubinin–Radushkevich can be represented as:

$$q_e = C_m \exp\left(-\beta\varepsilon^2\right) \tag{16}$$

3.6. Adsorption thermodynamics

The numerical values of thermodynamic parameters, that is, Gibbs free energy ($\Delta G°$), entropy ($\Delta S°$) and enthalpy ($\Delta H°$) for the adsorption of methylene blue and congo red were obtained with the help of van't Hoff equation and the related results are provided in Table 4.

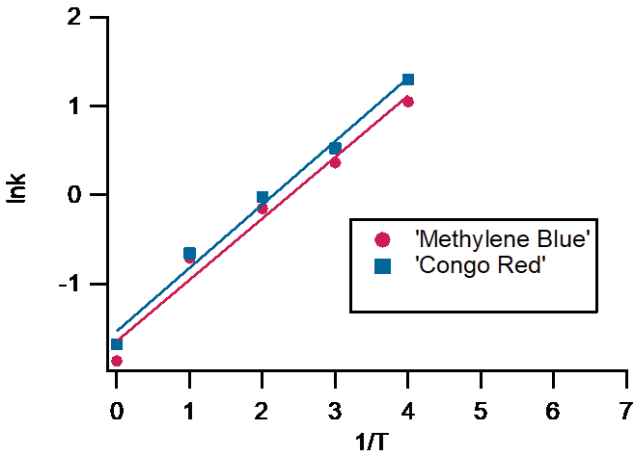

Fig. 14. Plot of $1/T$ vs. ln$K$ for the adsorption of methylene blue and congo red by SCB/CuO nanocomposite.

The graphical explanation for lnK_c vs. $1/T$ for these dyes is given in Fig. 14. Negative value of $\Delta G°$ represents the spontaneity of reaction while positive value of ΔH revealed that reaction was endothermic.

4. Conclusion

This article reveals the worth of SCB/CuO nanocomposite for the adsorptive removal of methylene blue and congo red by pseudo-second-order model showed better results with the kinetic experimental data as compared to other kinetic models. Thermodynamic parameters showed that adsorption of these dyes was exothermic process. Positive values of entropy showed that there is increase in randomness at adsorbate and adsorbent surface. The present research is highly efficient for the practicable synthesis of cost-effective, nanocomposites decontamination of organic pollutants from industrial effluents. From this study it was concluded that the SCB/CuO can be effectively used for the treatment of wastewater.

Conflict of interest

Authors declare no conflict of interest among them.

Funding

This research did not receive any specific grant from funding agencies in public, commercial, or not-for-profit sectors.

References

[1] O.S. Amuda, A.A. Giwa, I.A. Bello, Removal of heavy metal from industrial wastewater using modified activated coconut shell carbon, Biochem. Eng. J., 36 (2007) 174–181.
[2] X. Li, Y. Li, Adsorptive removal of dyes from aqueous solution by $KMnO_4$-modified rice husk and rice straw, J. Chem., 2019 (2019) 8359491, doi: 10.1155/2019/8359491.
[3] C.I. Pearce, J.R. Lloyd, J.T. Guthrie, The removal of colour from textile wastewater using whole bacterial cells: a review, Dyes Pigm., 58 (2003) 179–196.
[4] Y. Zhou, J. Lu, Y. Zhou, Y. Liu, Recent advances for dyes removal using novel adsorbents: a review, Environ. Pollut., 252 (2019) 352–365.
[5] N.J. Vickers, Animal communication: when i'm calling you, will you answer too?, Curr. Biol., 27 (2017) R713–R715.
[6] S. Wadhawan, A. Jain, J. Nayyar, S.K. Mehta, Role of nanomaterials as adsorbents in heavy metal ion removal from waste water: a review, J. Water Process Eng., 33 (2019) 101038, doi: 10.1016/j.jwpe.2019.101038.
[7] S. Ali, M. Rizwan, M.B. Shakoor, A. Jilani, R. Anjum, High sorption efficiency for As(III) and As(V) from aqueous solutions using novel almond shell biochar, Chemosphere, 243 (2020) 125330, doi: 10.1016/j.chemosphere.2019.125330.
[8] Qurat-Ul-Ain, M.U. Farooq, M.I. Jalees, Application of magnetic graphene oxide for water purification: heavy metals removal and disinfection, J. Water Process Eng., 33 (2020) 101044, doi: 10.1016/j.jwpe.2019.101044.
[9] M. Hassan, R. Naidu, J. Du, Y. Liu, F. Qi, Critical review of magnetic biosorbents: their preparation, application, and regeneration for wastewater treatment, Sci. Total Environ., 702 (2020) 134893, doi: 10.1016/j.scitotenv.2019.134893.
[10] M. Ahmad, A.U. Rajapaksha, J.E. Lim, M. Zhang, N. Bolan, D. Mohan, M. Vithanage, S.S. Lee, Y.S. Ok, Biochar as a sorbent for contaminant management in soil and water: a review, Chemosphere, 99 (2014) 19–33.
[11] X. Hu, Z. Ding, A.R. Zimmerman, S. Wang, B. Gao, Batch and column sorption of arsenic onto iron-impregnated biochar synthesized through hydrolysis, Water Res., 68 (2015) 206–216.
[12] Q. Fang, B. Chen, Y. Lin, Y. Guan, Aromatic and hydrophobic surfaces of wood-derived biochar enhance perchlorate adsorption via hydrogen bonding to oxygen-containing organic groups, Environ. Sci. Technol., 48 (2014) 279–288.
[13] M.I. Inyang, B. Gao, Y. Yao, Y. Xue, A. Zimmerman, A. Mosa, P. Pullammanappallil, Y.S. Ok, X. Cao, A review of biochar as a low-cost adsorbent for aqueous heavy metal removal, Crit. Rev. Env. Sci. Technol., 46 (2016) 406–433.
[14] Md. Ahmaruzzaman, Nano-materials: novel and promising adsorbents for water treatment, Asian J. Water Environ. Pollut., 16 (2019) 43–53.
[15] A.U. Rajapaksha, S.S. Chen, D.C.W. Tsang, M. Zhang, M. Vithanage, S. Mandal, B. Gao, N.S. Bolan, Y.S. Ok, Engineered/designer biochar for contaminant removal/immobilization from soil and water: potential and implication of biochar modification, Chemosphere, 148 (2016) 276–291.
[16] E. Meez, A. Rahdar, G.Z. Kyzas, Sawdust for the removal of heavy metals from water: a review, Molecules, 26 (2021) 4318, doi: 10.3390/molecules26144318.
[17] M.S. Sattar, M.B. Shakoor, S. Ali, M. Rizwan, N.K. Niazi, A. Jilani, Comparative efficiency of peanut shell and peanut shell biochar for removal of arsenic from water, Environ. Sci. Pollut. Res., 26 (2019) 18624–18635.
[18] N. Liu, Y. Zhang, C. Xu, P. Liu, J. Lv, Y. Liu, Q. Wang, Removal mechanisms of aqueous Cr(VI) using apple wood biochar: a spectroscopic study, J. Hazard. Mater., 384 (2020) 121371, doi: 10.1016/j.jhazmat.2019.121371.
[19] M.M. Nassar, E.A. Ashour, S.S. Wahid, Thermal characteristics of bagasse, J. Appl. Polym. Sci., 61 (1996) 885–890.
[20] A. Yadav, K.B. Ansari, P. Simha, V.G. Gaikar, A.B. Pandit, Vacuum pyrolysed biochar for soil amendment, Resour.-Effic. Technol., 2 (2016) S177–S185.
[21] M. Calvin, Solar energy by photosynthesis, Science, 184 (1974) 375–381.
[22] M.G. Rasul, V. Rudolph, M. Carsky, Physical properties of bagasse, Fuel, 78 (1999) 905–910.